SCIENCE CHINA
Technological Sciences

•Article•

February 2021 Vol.64 No.2: 297–316
https://doi.org/10.1007/s11431-019-1536-6

A deterministic FE contact analysis of 3D rough surfaces with textures and comparison with classic statistical contact models

ZHANG Rui[1], MENG XiangHui[1*], LYU BuGao[1] & SUN Kai[2]

[1]*School of Mechanical Engineering, Shanghai Jiao Tong University, Shanghai 200240, China;*
[2]*AECC Commercial Aircraft Engine Company Limited, Shanghai 200241, China*

Received October 27, 2019; accepted February 10, 2020; published online May 20, 2020

Accurate contact calculations of real rough surfaces are fundamental but complicated. The model-based methods are convenient and straightforward. But these methods ignore some factors and may lead to less accurate results. This is especially true when considering multi-scale topographic features of engineering rough surfaces. Based on artificially generated rough surfaces, the deterministic contact analysis of two 3D rough surfaces is conducted by the finite element method (FEM). The calculations show that when the separation between surfaces reduces, results of classic model-based methods are quite different from those of this study, especially when the roughness distribution and textures are considered. As friction pairs are working under increasing harsh conditions, the accurate contact calculation in this paper will be of great significance.

deterministic contact analysis, multi-scale topography, finite element method (FEM), engineering rough surfaces

Citation: Zhang R, Meng X H, Lyu B G, et al. A deterministic FE contact analysis of 3D rough surfaces with textures and comparison with classic statistical contact models. Sci China Tech Sci, 2021, 64: 297–316, https://doi.org/10.1007/s11431-019-1536-6

1 Introduction

With the development of equipment products, the working conditions of engineering friction pairs and the contact state between engineering rough surfaces are becoming more and more severe. In order to support the tribological design of engineering friction pairs, it is necessary to accurately evaluate the contact performance of the engineering rough surfaces at design stage. However, the accuracy of the contact computation faces many challenges. In particular, when the nominal separation between surfaces becomes very small under severer conditions, the multi-scale topographic features of surfaces, including roughness, texture, reticulation, and their distribution, have a significant impact on the contact performance. In order to make the calculation easy, most previous studies have adopted several assumptions to simplify the surface multi-scale features. However, this may lead to inaccurate results. Therefore, this paper will study the contact problem between two 3D rough surfaces with multi-scale topography and compare the results with those of previous methods.

There are two types of contact calculation methods in the academic field at present. One is the model-based methods, and the other is the numerical methods. The model-based methods are presented on the base of statistics or the fractal theory. Two pioneers in the field of tribology, Greenwood and Williamson [1], calculated the contact force between a rough surface and a rigid flat by using the statistical method and the Hertz contact theory [2]. Then Greenwood and Tripp [3] gave the contact calculation formula of two rough surfaces, namely the GT model. They proposed that two rough surfaces contact (two-rough-surface contact) can be equal to one equivalent single rough surface in contact with a rigid flat (equivalent single-rough-surface contact). Based on

*Corresponding author (email: xhmeng@sjtu.edu.cn)

these two models, Chang et al. [4] proposed the CEB model considering the transition of the contact state from pure elasticity to pure plasticity. Furthermore, Kogut and Etsion [5] obtained the critical point of elastic-plastic by carrying out a numerical simulation on the contact between an elastic-plastic sphere and a rigid flat. Then they studied the elastic-plastic change of the single-rough-surface contact and proposed the KE model [6]. As for the aspect of the fractal theory, Majumdar and Bhushan [7] believed that the rough surface conforms to the fractal characteristics and proposed the MB contact model. Persson [8] analyzed the amplification scale and introduced the fractal parameters for rough surfaces contact, and proposed the Persson model. Jackson and Streator [9] studied the normal contact problem of multi-scale rough surfaces based on the fractal theory. Furthermore, Miao and Huang [10] extended the modified asperity contact model to study a complete contact model of a fractal surface. They found that the critical area of a single asperity was scale dependent and that the asperity's plastic to elastic mode transition agreed with some classic contact mechanics. However, whether the fractal theory can accurately describe the rough surface of engineering friction pairs is still controversial. Meanwhile, it is also not easy to obtain the fractal parameters of an engineering rough surface. Among the model-based contact calculation methods, the GT model and the KE model are very classic and representative. The calculation formula of the mean contact pressure and the idea that two-rough-surface contact can be equal to its equivalent single-rough-surface contact have been widely adopted [11–13]. However, due to the assumptions made in the model-based methods, it may lead to less accurate results.

Compared with the model-based methods, the numerical methods release some assumptions and so may be more accurate in the contact calculation. The semi-analytical method, the boundary element method (BEM) and the finite element method (FEM) have been adopted to solve engineering contact problems. As for the semi-analytical method, the researchers usually put forward some new algorithms for special contact problems to release some assumptions of the full-analytic method. Therefore, the results will be more consistent with the real contact situation compared with the full-analytic method. Chen et al. [14] presented a 3D numerical elasto-plastic model for the contact of nominally flat surfaces, which can consider the effect of asperity interactions. Their model is built on two algorithms: the continuous convolution and Fourier transform (CC-FT) and discrete convolution and fast Fourier transform (DC-FFT). Zhang et al. [15] studied the influence of the kurtosis and the skewness on the elastic-plastic contact performance of rough surfaces based on the minimization of complementary energy and semi-analytical method. Zhao et al. [16] used the semi-analytical and numerical method to study the sliding asperity interaction for the power-law hardening materials. Considering the wide application of surface coatings, Nyqvist et al. [17] presented a new semi-analytical model for analysis of non-conformal rough surface contacts where one or both of the contacting bodies are coated with a multilayered coating.

In the study of the BEM for contact calculation of engineering rough surfaces, some researchers conducted the calculation based on the half-space assumption. Therefore, the subjects of the BEM are usually the high friction pairs, and the equivalent operation is commonly used. Peng and Bhushan [18] used BEM to study the problem that a small rough surface in sliding contact with a layered surface. To make the calculation easier, Bemporad and Paggi [19] reviewed the fundamental equations for the solution of the frictionless unilateral normal contact problem between a rough rigid surface and a linear elastic half-plane using the BEM. Besides, considering the adhesive properties of rough surfaces, Rey et al. [20] proposed a numerical method to compute the solution of an adhesive normal contact problem. However, the elastic half-space assumption commonly used in the BEM, which is usually valid in high friction pairs, is often no longer applicable in the case of low friction pairs. Meanwhile, although the computing scale of the BEM is smaller than that of the FEM, the BEM method does not apply to non-homogeneous and nonlinear problems. So the BEM is not as accurate as the FEM when describing local characteristics of complicated rough surfaces.

Compared with the BEM method, the FEM may be more accurate but the calculation cost may be a problem. Based on the FEM, Jackson and Green [21] studied an elasto-plastic hemispherical contact against a rigid flat, and concluded that the hardness will change with the contact geometry and materials. In their research, the hemisphere is regarded as an asperity, so it is far from the contact calculation of rough surfaces. It has long been believed that the use of the FEM to simulate the contact between rough surfaces is not possible because the cost will be very high when considering a huge amount of roughness or asperities. However, along with the development of computers and high-performance computing algorithm, the cost is no longer an obstacle. So in recent years the FEM has been found to solve the contact problems of engineering rough surfaces [22–24]. Generally, there are two methods to obtain the rough surface data for the FEM calculation. One is collecting the measured surface data directly, and the other is using some algorithms to generate a rough surface. Zhao et al. [25] studied the contact of rough surfaces for power-law hardening materials with measured surface data by the FEM. Using the measured surface data is more practical, but it is less efficient and convenient. The method of generating a rough surface with a particular algorithm can quickly obtain a rough surface that meets specific statistical parameters requirements. This makes the method more convenient, especially for the comparison of

the results of the FEM with those of the model-based methods. The digital generation methods of Gaussian and non-Gaussian rough surfaces were studied in refs. [26–28]. Besides, some FE analysis about the contact between a rigid flat and a self-affine fractal rough surface based on fractal theory were also discussed in refs. [29,30]. Recently, more and more researchers use the FEM to study the deterministic contact between rough surfaces. Poulios and Klit [31] used FEM to study the deterministic frictionless contact between nominally flat rough surfaces. Their surface topographies were numerically generated combined with the roughness measured by a stylus instrument. Besides, An et al. [32] used measured surfaces to conduct the deterministic elastic-plastic modelling of rough surfaces and compared their results with some model-based methods based on the fractal theory. When adopting the FEM to deal with the contact problem of rough surfaces, the distribution and the mutual influence of asperity peaks and the multi-scale topography features can be considered. Therefore, using the FEM can establish a deterministic contact model, which means that the method can be used for contact problems between engineering rough surfaces with multi-scale topography.

This paper will consider the multi-scale topographic features and their distributions of engineering surfaces to reach a deterministic contact analysis. Based on the FEM, the contact of two rough surfaces will be analyzed. Moreover, in order to further discuss the relevant characteristics of rough surface contact for more accurate conditions, the results in this study will be compared with those calculated by the classic model-based methods.

2 Deterministic contact analysis

2.1 Generation of 3D rough surfaces

Before conducting the deterministic contact analysis, it is necessary to obtain the 3D rough surfaces firstly. Compared with the measurement of engineering rough surfaces, the generation of rough surfaces using particular algorithm can quickly obtain rough surfaces with specific statistical parameters. This will be beneficial for the comparison of the results in this study with those of the traditional model-based methods. So the generated rough surfaces will be used in this study. Poon and Bhushan [33] have presented a generation method of Gaussian rough surfaces. Hu and Tonder [34] have presented a generation method of non-Gaussian rough surfaces by the Johnson transition system. However, these methods can only generate a Gaussian surface or a non-Gaussian surface with specific roughness σ, which is far away to describe a rough surface accurately. So, based on these previous works, this paper gives a convenient computing method which can generate a Gaussian 3D rough surface with specific parameters η, β and σ. Then, textures can be introduced into the generated rough surface to obtain a multi-scale rough surface, which is common in engineering friction pairs. The flow chart of generating a Gaussian 3D rough surface with specific parameters η, β and σ is shown in Figure 1 (see Appendix A for the specific process).

The method of generating a Gaussian 3D rough surface with specific parameters η, β, σ is based on the generation of white noise and the selection of autocorrelation function (ACF). On the one hand, by taking discrete Fourier transform (DFT) of the initial matrix, the corresponding Fourier matrix $A(m,n)$ can be obtained. On the other hand, after the discretization and DFT, the transfer function matrix $H(m,n)$ can be obtained. Then, by taking inverse Fourier transform of $(A \cdot H)$ and modification, the Gaussian rough surface matrix $z(m,n)$ that meets the given standard deviation requirement is obtained. Furthermore, it is necessary to confirm whether the rough surface matrix $z(m,n)$ satisfies the η, β requirements and Gaussian distribution. If it does not satisfy the η, β requirements, the input parameters of ACF should be modified. While if $z(m,n)$ does not satisfy the Gaussian distribution, it is necessary to regenerate the initial matrix

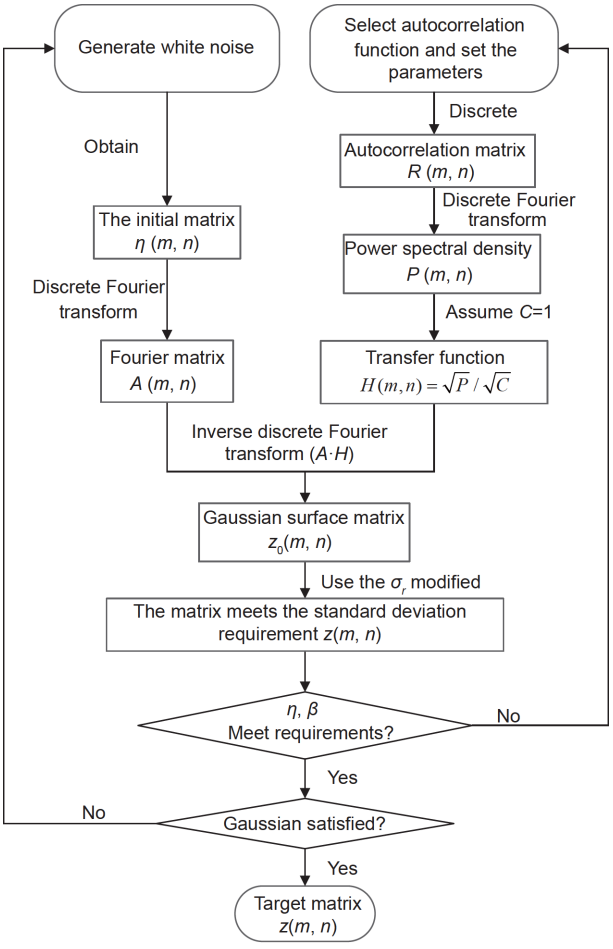

Figure 1 The flow chart of generating the Gaussian 3D rough surface with specific parameters η, β and σ.

$\eta(m,n)$. Besides, considering the randomness of the initial matrix, each group of input parameters can be repeated for many times when performing the operations shown in Figure 1. The ACF selected in this paper is

$$f(x,y)=\sigma_{\text{input}}^2 e^{-2.3\sqrt{\left(\frac{x}{L_x}\right)^2+\left(\frac{y}{L_y}\right)^2}}. \tag{1}$$

Using this ACF, the desired output parameters can be controlled by adjusting the standard deviation σ_{input} and the autocorrelation length L_x, L_y. This paper considers isotropic surfaces, so set L_x=L_y. And if the anisotropic surface is wanted to be obtained, the L_x and L_y should be not equal. When $L_x/L_y>1$, the surface will appear the characteristic that along the partial x direction, and vice versa. This trend will become more obvious as the ratio increases. The relative properties of anisotropic surfaces, such as friction, show significant directional differences. Therefore, the direction should be taken into consideration when contact problems of anisotropic surfaces are studied.

The detail relationship between input and output parameters are as follows: (1) The output roughness σ is positively correlated with the σ_{input}; (2) When L_x, L_y are constant, β is inversely correlated with σ_{input}, while σ_{input} have no significant effect on η; (3) When σ_{input} is constant, η is inversely correlated with L_x, L_y, while β is positively correlated with L_x, L_y. Besides, it is worth noting that the detailed change trend is also related to the computing expression of η, β. Considering that the commonly method [35] used to calculate the η, β is one-dimension, which means it is not accurate to deal with the 3D rough surface problem. Therefore, the method in ref. [25] can be referred here. As shown in Figure 2, when a point of the matrix $z(m,n)$ satisfies

$$z(i,j)>z(u,v), \tag{2}$$

where u=i–2, i–1,…, i+2, v=j–2, j–1,…, j+2 except (i,j)=(u,v), then this point is regarded as an asperity peak. After judging each point of the rough surface, the η can be obtained:

$$\eta=\frac{N}{A_n}, \tag{3}$$

where N is the number of asperities on the whole rough surface. The calculation of radius of the corresponding single asperity peak can be calculated as follows:

$$\begin{cases}\beta_x=\dfrac{\left[1+(z'(x))^2\right]^{\frac{3}{2}}}{z''(x)},\\ \beta_y=\dfrac{\left[1+(z'(y))^2\right]^{\frac{3}{2}}}{z''(y)},\\ \beta_s=\sqrt{\beta_x\beta_y}.\end{cases} \tag{4}$$

Then, the β can be obtained by the following expression:

$$\beta=\frac{\sum_{i=1}^{N}\beta_s(i)}{N}. \tag{5}$$

When judging the asperity peak, the determination is whether the point is larger than the surrounding 24 points, which means the whole range is 4 μm. Considering the size of the entire analysis region is 63 μm×63 μm, it is believed that this range is reasonable in this paper. In other cases, the size of the judging range can be modified according to the specific situation.

One example of the rough surface data, which meets all requirements and has a particular asperity distribution, is shown in Figure 3. The height distribution of the rough surface and the Gaussian fitting are shown in Figure 4.

Based on the generated rough surface with specific parameters η, β, σ, textures can be added according to some purpose to obtain a multi-scale 3D rough surface. In this paper, a common dimple texture is introduced into the center

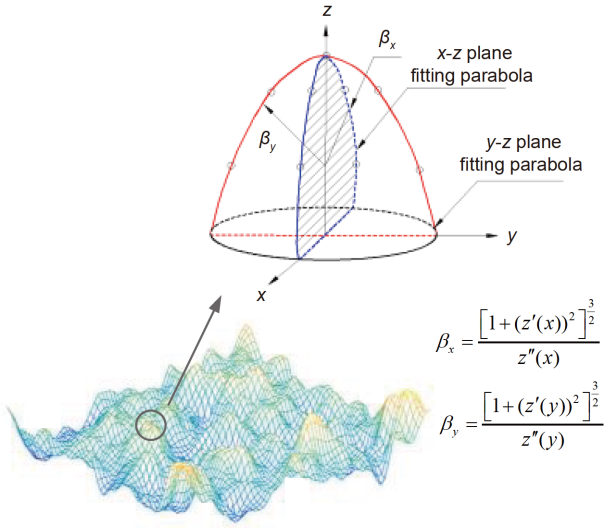

Figure 2 (Color online) Schematic of the formula to determine the radius of asperity peak in x-z plane and y-z plane.

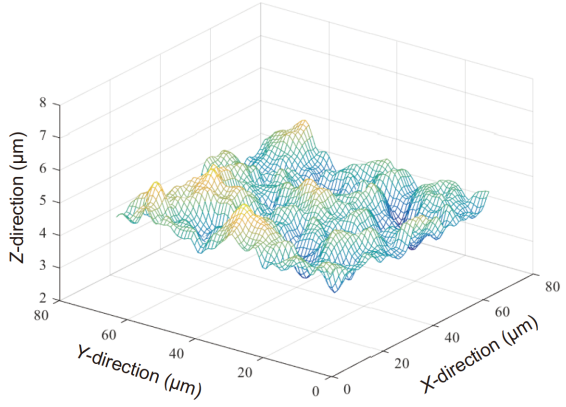

Figure 3 (Color online) The rough surface data that meets all requirements and has a particular asperity distribution.

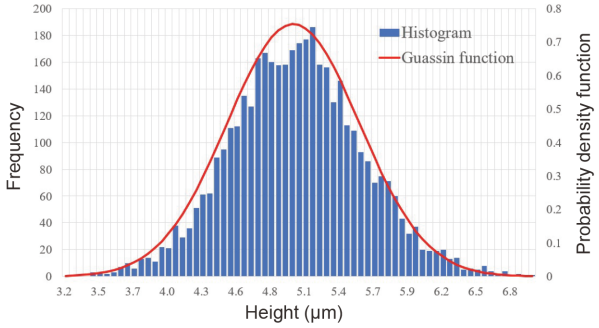

Figure 4 (Color online) The height distribution of rough surface and Gaussian fitting.

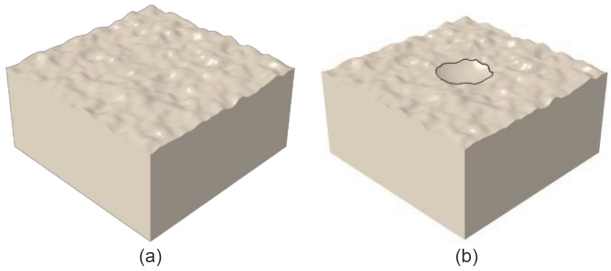

Figure 5 (Color online) 3D rough solid. (a) Rough surface; (b) rough surface with texture.

of the lower rough surface. The diameter of the dimple texture is 30 μm, and the depth is 3 μm. The 3D rough surfaces with solid base namely the 3D rough solid, are shown in Figure 5. And the schematic diagram of the dimple texture is also shown in Figure 6.

2.2 Mesh generation and validation by the FEM

Based on the artificially generated surfaces in Section 2.1, the FE model can be obtained as shown in Figure 7. The size of the single 3D rough solid is 63 μm×63 μm×30 μm. In the x and the y directions, the meshing size is 0.5 μm. Hence, the number of the elements on the surface is approximately 126×126. According to ref. [36], sparse processing is carried out in the z direction, which is divided into 10 layers. In order to ensure the reliability of the simulation results, the mesh convergence test is carried out. The meshing size is reduced from 1 to 0.25 μm. Figure 8 presents the dimensionless contact load versus the dimensionless separation. It can be seen that, when the meshing size is reduced to 0.5 μm, the results are not significantly different. The corresponding relative error is also shown in Figure 9. Compared with the convergency test in ref. [37], the relative error in this paper has been controlled to be small enough, which means the meshing size 0.5 μm is reasonable in this paper. And the computation time is also listed in Table 1.

In addition, considering the reasonable choice of the thickness of the 3D rough solid is important. The test about the thickness is also carried out in this paper. The thickness increases from 20 to 40 μm. Figure 10 presents the dimensionless contact load versus the dimensionless separation. It can be seen that, when the thickness increases to 30 μm, the results are very close to those of 40 μm. The corresponding relative error is also shown in Figure 11. As shown in Figure 11, the relative error of the results for thickness of 30 μm to those for thickness of 40 μm is around 2%.

2.3 Loads, boundary conditions and contact algorithm

As shown in Figure 12, the loads and boundary conditions are added into the contact bodies as follows: (1) displacement load is applied on the top surface of the upper solid, while the displacement of the upper solid in the x and y directions is constrained; (2) all degrees of freedom of the lower solid are restricted on the bottom surface. In order to ensure better precision, the contact algorithm is the "finite sliding algorithm" in this paper. Following the GT and the KE model where the smooth Hertz contact model is adopted, the interface between two contacting surfaces is assumed to be frictionless during the normal contact.

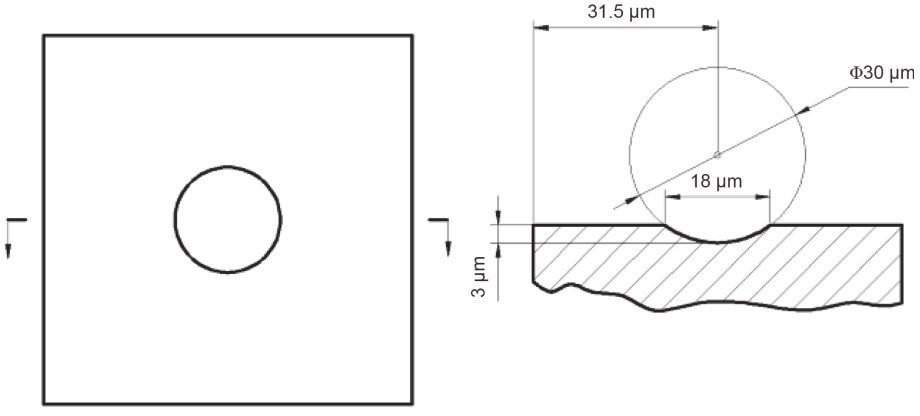

Figure 6 The schematic diagram of the dimple texture.

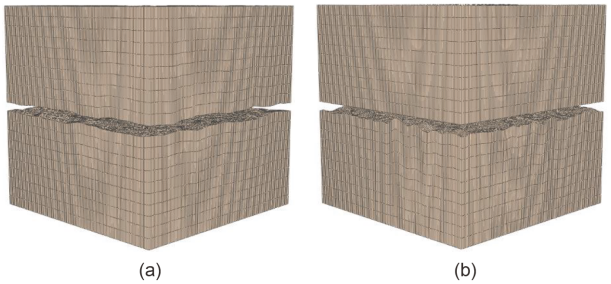

Figure 7 (Color online) The FE model for (a) two-rough-surface contact and (b) single-rough-surface contact.

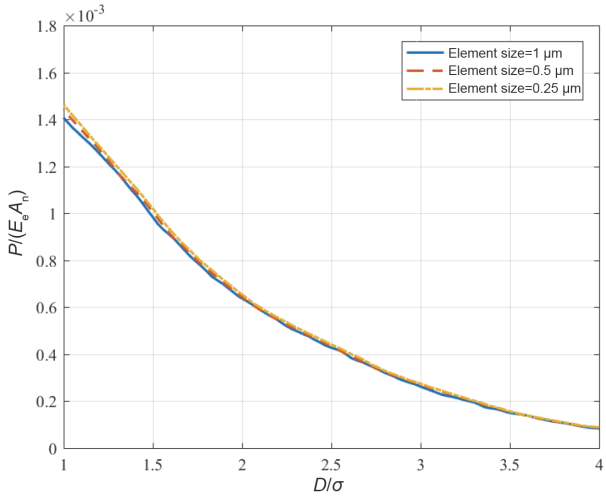

Figure 8 (Color online) The test of mesh convergency.

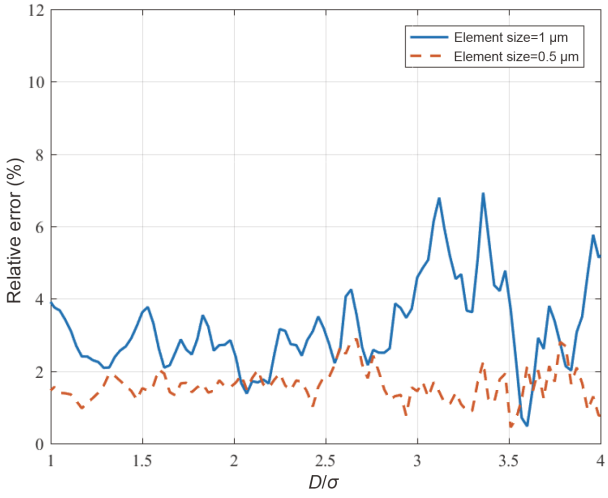

Figure 9 (Color online) The relative error to the results of the element size=0.25 μm.

3 Material properties

In this paper, the contact body is assumed the basic material S235. Some properties of the S235 are shown in Table 2 [38]. As shown in Figure 13, considering that the stress-strain curve in ref. [38] is engineering stress-strain, it is necessary to convert it into the true stress-strain data. The transformation process is as follows.

The engineering strain during compression is

$$\varepsilon = \frac{H_{\text{inital}} - H_{\text{now}}}{H_{\text{inital}}} = 1 - \frac{H_{\text{now}}}{H_{\text{inital}}}, \tag{6}$$

where H_{inital}, H_{now} are the initial length and the current length, respectively.

Table 1 The computation time

Element size (μm)	Time	CPU brand	Multiple processors	Memory (GB)
1	3h20min	Intel core i7-8700 @ 3.20 GHz	6	24
0.5	20h25min	Intel core i7-8700 @ 3.20 GHz	6	24
0.25	11d4h42min	Intel core i7-8700 @ 3.20 GHz	6	24

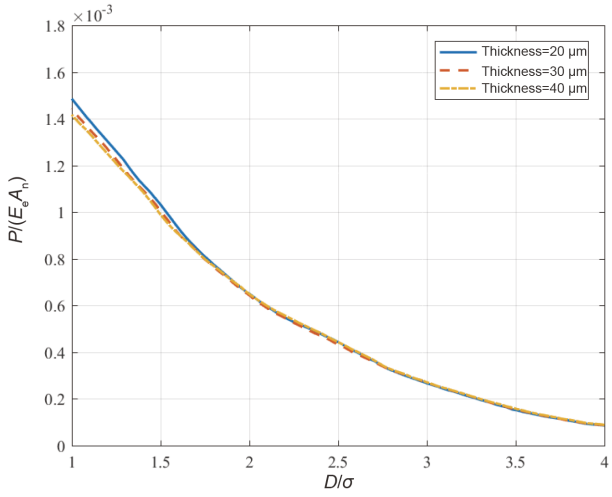

Figure 10 (Color online) The test of thickness.

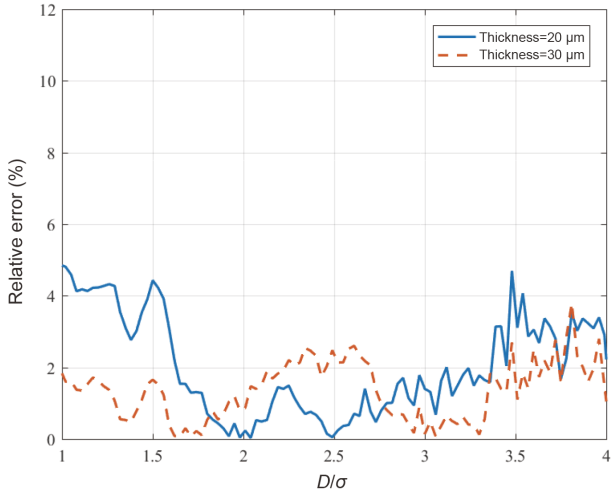

Figure 11 (Color online) The relative error to the results of the thickness=40 μm.

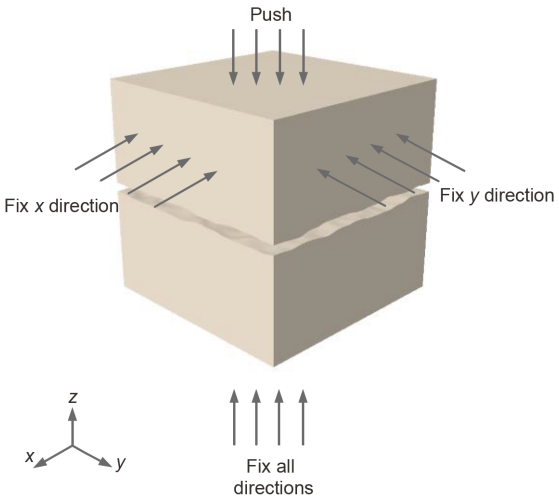

Figure 12 (Color online) Schematic of loading form and boundary condition.

Table 2 Material properties of S235

Quantity	Value
Elastic modulus E (GPa)	203
Yield strength S_y (MPa)	235
Density ρ (kg/m^3)	7850
Poisson's ratio v	0.3

Then the true strain is

$$\varepsilon_t = \ln\left(\frac{H_{\text{inital}}}{H_{\text{now}}}\right) = \ln\left(\frac{1}{1-\varepsilon}\right). \tag{7}$$

Based on the principle of volume invariance

$$A_{\text{inital}}H_{\text{inital}} = A_{\text{now}}H_{\text{now}} = \text{const.} \tag{8}$$

The current area is

$$A_{\text{now}} = A_{\text{inital}}\frac{H_{\text{inital}}}{H_{\text{now}}} = A_{\text{inital}}\frac{1}{1-\varepsilon}. \tag{9}$$

Therefore, the true stress is

$$\sigma_{\text{t}} = \frac{P}{A_{\text{now}}} = \frac{P}{A_{\text{inital}}}(1-\varepsilon). \tag{10}$$

The final true stress-strain is shown in Figure 13.

4 Comparison with classic contact models

From the analysis procedure and the generated 3D rough surfaces in Section 2, a deterministic contact analysis can be conducted. To show the deterministic contact results more clearly, two classic model-based methods, the GT model and the KE model, are adopted to make the comparison.

4.1 Classic contact models

Before accurately considering the rough surfaces with multi-scale topographic features such as textures and roughness in the contact calculation, this paper reviews two classic model-based contact models, the GT model and the KE model. Some issues will be analyzed for a better comparison later.

4.1.1 GT model

The GT model is based on some assumptions [39]. Some important assumptions are (1) there is no interaction between separate asperities; (2) the height distribution of rough surface is Gaussian; (3) the contact analysis of the two-rough-surface contact could be equal to its equivalent single-rough-surface contact. According to the GT model, the equivalence requirements are below [36]:

$$\begin{cases} \eta_1+\eta_2=\eta, \\ \dfrac{1}{\beta_1}+\dfrac{1}{\beta_2}=\dfrac{1}{\beta}, \\ \sigma_1^2+\sigma_2^2=\sigma^2, \end{cases} \tag{11}$$

where η_1, η_2 are the areal asperity density, β_1, β_2 mean the radius of asperity peaks, and σ_1, σ_2 are the standard deviation of surface height for two different rough surfaces respectively. While η, β, σ are the corresponding surface parameters of the equivalent single-rough-surface. The expression of the contact load [39] is

$$P(d) = 2\pi\eta^2 A_n \int_z\int_r P\left(\omega_{\text{p}}-\frac{r^2}{4\beta}, r\right)\phi(z)r\,\mathrm{d}r\,\mathrm{d}z. \tag{12}$$

By defining the integral against r, the above expression can be decomposed into the following expression:

$$\begin{cases} P(d) = \eta A_n \displaystyle\int_d^{\infty} P_0(z-d)\phi(z)\mathrm{d}z, \\ P_0(\omega_{\text{p}}) = 2\pi\eta\displaystyle\int_r P\left(\omega_p-\frac{r^2}{4\beta}, r\right)r\mathrm{d}r. \end{cases} \tag{13}$$

It can be found that the GT model considers the dislocation contact between asperity peaks for the two-rough-surface contact by integrating twice. The mean contact pressure of the two-rough-surface contact is

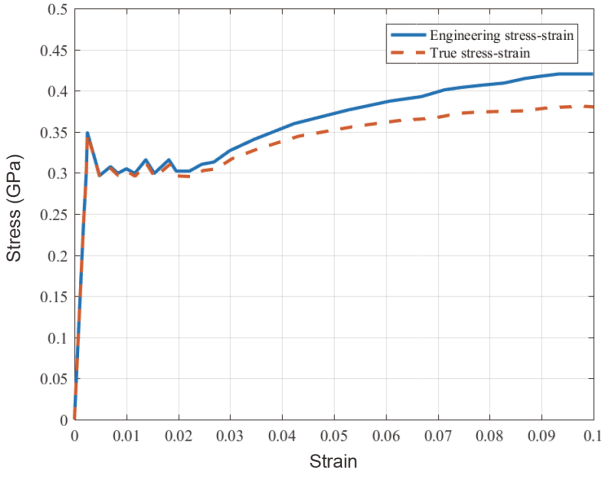

Figure 13 (Color online) The curve of stress-strain.

$$p(d) = \frac{8\pi\eta\beta\sigma}{5} KF_{2.5}\left(\frac{d}{\sigma}\right), \tag{14}$$

where

$$K = \frac{2\sqrt{2}\eta\beta\sigma E_e}{3}\sqrt{\frac{\sigma}{\beta}},$$

$$E_e = 1/\left[\left(1-\nu_1^2\right)/E_1 + \left(1-\nu_2^2\right)/E_2\right]$$

is the equivalent elastic modulus, $F_n(d/\sigma)$ is a calculation formula related to the height distribution. The specific calculation and results of $F_n(d/\sigma)$ are shown in Appendix B. The contact area formula of the two-rough-surface contact can also be obtained by quadratic integration:

$$A_r = \pi^2(\eta\beta\sigma)^2 A_n F_2\left(\frac{d}{\sigma}\right). \tag{15}$$

For the equivalent single-rough-surface contact, the mean contact pressure formula is

$$p(d) = KF_{1.5}\left(\frac{d}{\sigma}\right). \tag{16}$$

By comparing eqs. (14) and (16), it can be seen that the differences between these two formulas are the coefficient and the F function, which results from the quadratic integration.

It might as well set that $\eta\beta\sigma$=0.05, K=100 MPa, E_e =110 GPa for a detailed analysis. The influence of F on the results is shown in Figure 14, in which the value of F of the two-rough-surface is about 1–1.5 times of that of the equivalent single-rough-surface. Meanwhile, the coefficient $8\pi\eta\beta\sigma/5$ is about 0.2513 in this condition. Generally speaking, it means that in the GT model, the dimensionless contact load of the equivalent single-rough-surface contact is 2.5–3 times larger than that of the two-rough-surface contact. The dimensionless contact load versus dimensionless separation is shown in Figure 15. Obviously, the operation in the GT model which considers the influence of dislocation contact through quadratic integration form has a significant effect on the prediction of the contact load.

4.1.2 KE model

As shown in Figure 16, Kogut and Etsion [5] made a distinction between the mean height of the surface D and that of

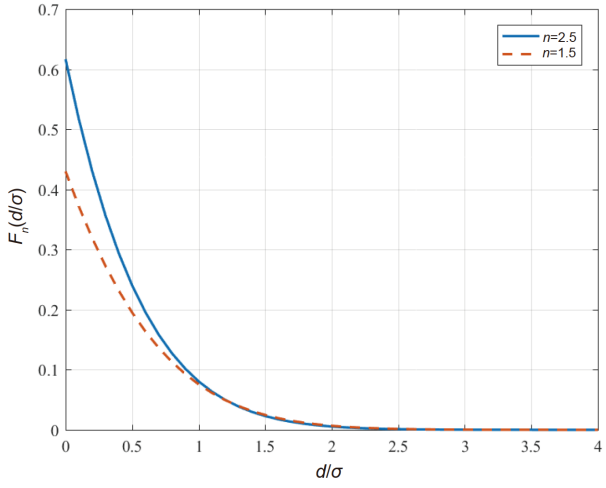

Figure 14 (Color online) The data of $F_n(d/\sigma)$.

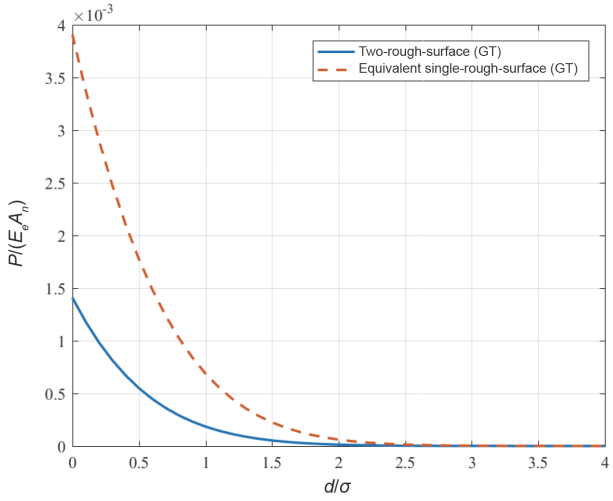

Figure 15 (Color online) Comparison of dimensionless contact load versus dimensionless separation.

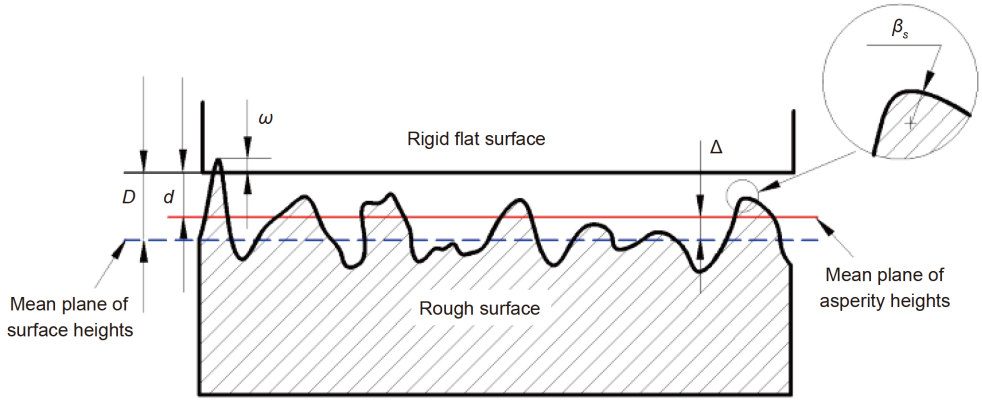

Figure 16 (Color online) Contacting rough surfaces in KE model.

the asperities d in the KE model. Then they presented the contact calculation formulas considering the elastic and plastic deformation between a rough surface and a rigid flat surface.

The following parameters with superscript * mean that these parameters are dimensionless by the σ. Expressions of the critical interface and the corresponding dimensionless parameters are below:

$$\begin{cases} \omega_c = \left(\dfrac{\pi KH}{2E_e}\right)^2 \beta, \\ \omega_c^* = \dfrac{\omega_c}{\sigma} = \left(\dfrac{\pi KH}{2E_e}\right)^2 \dfrac{\beta}{\sigma}, \end{cases} \tag{17}$$

where K=0.454+0.41ν, H=2.8S_y, S_y means the yield strength of the material. The calculation expression of the mean contact pressure in the KE model is as follows (see Appendix C for the specific process):

$$\begin{aligned} p(d^*) = {} & \frac{2}{3} KH\,\pi\times \eta\beta\sigma \\ & \times\left\{(\omega_c^*)^{-0.5}\left[F_{1.5}(d^*) - F_{1.5}(d^*+\omega_c^*)\right]\right. \\ & +1.03(\omega_c^*)^{-0.425} \\ & \times\left[F_{1.425}(d^*+\omega_c^*) - F_{1.425}(d^*+6\omega_c^*)\right] \\ & +1.4(\omega_c^*)^{-0.263} \\ & \times\left[F_{1.263}(d^*+6\omega_c^*) - F_{1.263}(d^*+110\omega_c^*)\right] \\ & \left.+\frac{3}{K}F_1(d^*+110\omega_c^*)\right\}. \end{aligned} \tag{18}$$

While the contact area formula is

$$\begin{aligned} A_r(d^*) = {} & \pi\times\eta\beta\sigma\times A_n\left\{\left[F_1(d^*) - F_1(d^*+\omega_c^*)\right]\right. \\ & +0.93(\omega_c^*)^{-0.136} \\ & \times\left[F_{1.136}(d^*+\omega_c^*) - F_{1.136}(d^*+6\omega_c^*)\right] \\ & +0.94(\omega_c^*)^{-0.146} \\ & \times\left[F_{1.146}(d^*+6\omega_c^*) - F_{1.146}(d^*+110\omega_c^*)\right] \\ & \left.+2F_1(d^*+110\omega_c^*)\right\}. \end{aligned} \tag{19}$$

Because the plastic deformation is considered, the prediction of the mean contact pressure of the KE model is smaller than that of the GT model at the later contact stage. The detailed comparison results are shown in Section 4.3.

4.2 Dimensionless separation

Dimensionless separation, such as d/σ in eq. (16) or d^* in eq. (18), is a very important parameter in both the GT model and the KE model. However, when comparing the results of different methods, the dimensionless separation must be carefully processed to make the results comparable.

When directly using the function $F_n(d/\sigma)$, the variable is the dimensionless separation corresponding to the rough surface σ. However, different surfaces have different σ. In this situation, when comparing the results of two contact cases, in which the σ is different, it will be reasonable to select the same value of σ. Taking the situation in Figure 17 as an example, it may as well suppose that σ_a=2σ_b, where σ_a is the composite roughness of contact case 1 and σ_b is the composite roughness of contact case 2. When the dimensional separations in two cases are the same, for example, it is equal to 2σ_a, the dimensionless separation in case 1 will be half of that in case 2 if different roughness are used for dimensionless calculation. To compare the contact performance of two cases in one figure, it is better to use the same roughness, such as σ_a, for dimensionless calculation.

Another problem is that the definition of the separation. As the discussion in the KE model, the separation D based on surface heights is different from the separation d based on asperity heights. Therefore, when comparing the simulation results with the results of the GT model and the KE model, the separation needs to be modified to be the same. As shown in Figure 18, for the single-rough-surface contact, the modification Δ_s is one-sided, while for the two-rough-surface contact, the modification Δ_d is two-sided.

4.3 Comparison between the deterministic analysis and the model-based analysis

Here the 3D rough surface parameters listed in Table 3 will be adopted to conduct the deterministic analysis. While the corresponding σ, β, η used in the GT model and the KE model are listed in Table 4. The calculation of equivalent surface parameters follows eq. (11). And formulas used to calculate the GT model are the formulas for two-rough-

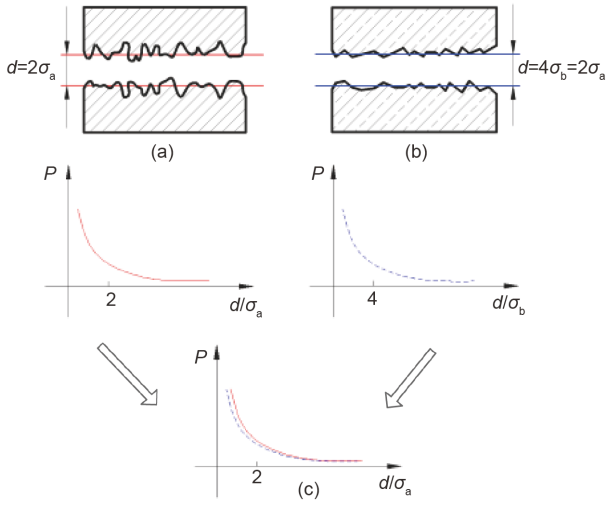

Figure 17 (Color online) Schematic of separation dimensionless processing. (a) Contact case 1; (b) contact case 2; (c) contact load versus dimensionless separation of case 1 and case 2.

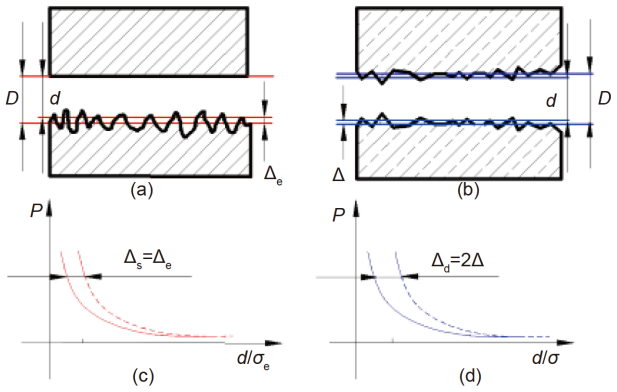

Figure 18 (Color online) Schematic of separation modification. (a) The single-rough-surface contact; (b) the two-rough-surface contact; (c) contact load versus dimensionless separation of the single-rough-surface contact; (d) contact load versus dimensionless separation of the two-rough-surface contact.

surface contact. It can be seen from Table 2 that deviation between composite values of the two-rough-surface and values of the equivalent rough surface are very small. And modified separations are shown in Table 5, which can be obtained by post-processing of the data in Section 2.1. The 3D rough solids and rough surface data are also shown in Figure 19.

Figure 20(a) presents the dimensionless contact load versus the dimensionless separation, in which σ_e of the equivalent single-rough-surface is used for the dimensionless processing. At the early stage of the contact, the results of the deterministic analysis are similar to the GT model and the KE model, no matter for the two-rough-surface contact or the equivalent single-rough-surface contact. However, when the dimensionless separation d/σ_e reduces to about 1.5, the results begin to differ significantly. It should be noticed that the results of the KE model is closer to that of the deterministic results than that of the GT model.

Figure 20(b) presents the contact area ratio versus the dimensionless separation. It can be seen that the predicted results of the GT model is obviously smaller than that of the KE model and the deterministic results. Similar to the dimensionless contact load results, the contact area ratio of the KE model is closer to the deterministic results than the GT model, especially to the deterministic results of the equivalent single-rough-surface contact. Comparing eq. (15) with eq. (19), it can be seen that the contact area formula of the GT model has an extra coefficient $\eta\beta\sigma$ due to the quadratic integration. Considering that the value of $\eta\beta\sigma$ is usually between 0.03–0.05, the effect of the coefficient is significant. The dislocation contact between peaks may really exist. As shown in Figure 20, the results of the two-rough-surface contact are both smaller than those of the equivalent single-rough-surface at the later stage, which can confirm the idea of dislocation contact. However, the effect of the coefficient introduced by the quadratic integration seems too significant.

Table 3 Summary of surface parameters for deterministic analysis

Type	Surface	σ (μm)	β (μm)	η (mm^{-2})
Two-rough-surface	Rough surface 1	0.3668	7.4649	9070
	Rough surface 2	0.3668	7.4649	9070
	Composite surface	0.5187	3.7325	18140
Equivalent single-rough-surface	Rigid flat surface	–	–	–
	Equivalent rough surface	0.5295	3.7196	18392
Deviation	–	2.09%	0.34%	1.39%

Table 4 Summary of surface parameters for the KE model and the GT model

Type	Surface	σ (μm)	β (μm)	η (mm^{-2})
GT model	Rough surface 1	0.3668	7.4649	9070
	Rough surface 2	0.3668	7.4649	9070
	Composite surface	0.5187	3.7325	18140
KE model	Rigid flat surface	–	–	–
	Equivalent rough surface	0.5187	3.7325	18140

Table 5 Rough surface modified separation

Type	Δ (μm)	Δ_{all} (μm)
Two-rough-surface contact	0.4412	0.8824
Single-rough-surface contact	0.6830	0.6830

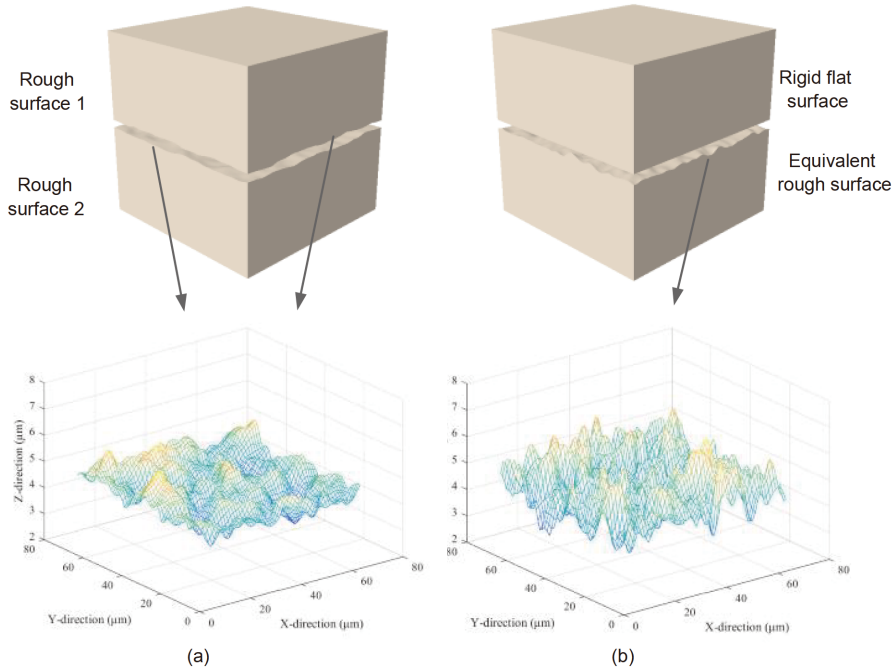

Figure 19 (Color online) The rough surface contact (a) deterministic two-rough-surface contact, and (b) deterministic equivalent single-rough-surface contact.

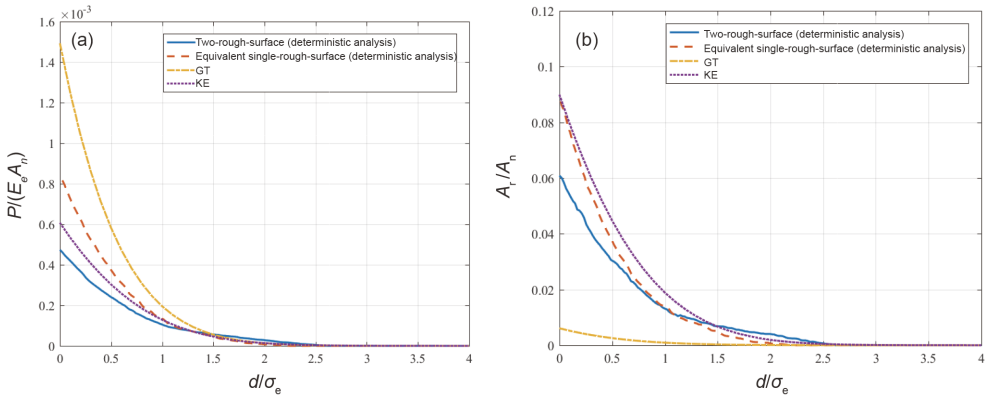

Figure 20 (Color online) Comparison of dimensionless contact load (a) and contact area ratio (b) versus dimensionless separation.

The specific analysis will be carried out in the next.

By comparing the prediction results of the GT model with the deterministic results, it can be seen that the dimensionless contact load of the GT model at the later contact stage are obviously larger than that of the deterministic contact. It is mainly because the plastic stage is not considered in the GT model. As a comparison, the results of the KE model, in which both the elastic and the plastic deformation have been considered, are more consistent with the deterministic results than that of the GT model. At the later stage, it is interesting to notice that the dimensionless contact load value of the KE model is smaller than that of the deterministic equivalent single-rough-surface contact while greater than that of the deterministic two-rough-surface contact. The KE model is also based on the assumption of the equivalent single-rough-surface contact. So, the critical parameters in the KE model may be the reason why its dimensionless contact load is smaller than that of the deterministic equivalent single-rough-surface contact. It is well known that the critical parameters in the KE model are derived based on the analysis of single asperity. However, in actual contact, the radius and height of each asperity are quite different. The higher asperities will come into contact earlier, while the lower asperities will come into contact later. Therefore, the critical value given by the KE model based on statistics may be inaccurate. Meanwhile, the predicted dimensionless contact load of the KE model is greater than that of the deterministic two-rough-surface contact. This phenomenon may because

that the effect of dislocation contact is not considered in the KE model. Therefore, the dislocation coefficient should be introduced into the KE model.

To make more comparisons between the deterministic rough surface contact and the model-based methods, the other two sets of rough surface contact in different σ, β, η cases are also carried out. The surface parameters of the new case A and case B are listed in Table 6. And the results are shown in Figures 21 and 22. It can be seen that the new deterministic results have the similar tendency with the previous results shown in Figure 20. Although the KE model considered the plastic stage, the results of the KE model are still have some differences with results of the deterministic rough surface contact.

And it is interesting to notice that, in the case A, as shown in Figure 21(a), there exists a small mutation of the dimensionless contact load of the deterministic two-rough-surface contact, when the dimensionless separation reduces

Table 6 Summary of surface parameters in case A and case B

Case	Type	Surface	σ (μm)	β (μm)	η (mm^{-2})
Case A	Two-rough-surface contact	Rough surface 1	0.2986	9.4683	9238
		Rough surface 2	0.2986	9.4683	9238
		Composite surface	0.4223	4.7341	18476
	Equivalent single-rough-surface	Rigid flat surface	–	–	–
		Equivalent rough surface	0.4217	4.7872	18087
	Deviation	–	0.15%	1.12%	2.10%
	GT model	Rough surface 1	0.2986	9.4683	9238
		Rough surface 2	0.2986	9.4683	9238
		Composite surface	0.4223	4.7341	18476
	KE model	Rigid flat surface	–	–	–
		Equivalent rough surface	0.4223	4.7341	18476
Case B	Two-rough-surface contact	Rough surface 1	0.4014	8.0691	8715
		Rough surface 2	0.4014	8.0691	8715
		Composite surface	0.5676	4.0346	17430
	Equivalent single-rough-surface	Rigid flat surface	–	–	–
		Equivalent rough surface	0.5633	4.0120	17123
	Deviation	–	0.76%	0.56%	1.76%
	GT model	Rough surface 1	0.4014	8.0691	8715
		Rough surface 2	0.4014	8.0691	8715
		Composite surface	0.5676	4.0346	17430
	KE model	Rigid flat surface	–	–	–
		Equivalent rough surface	0.5676	4.0346	17430

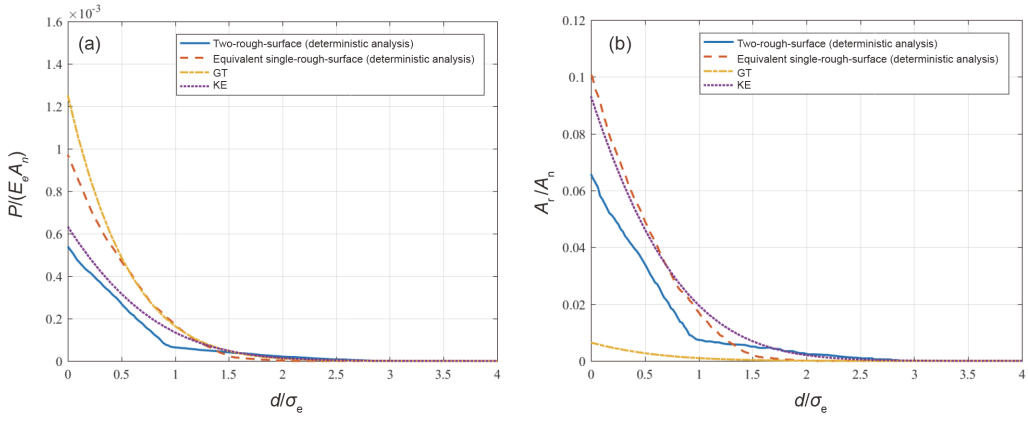

Figure 21 (Color online) Deterministic analysis in case A. (a) Dimensionless contact load versus dimensionless separation; (b) contact area ratio versus dimensionless separation.

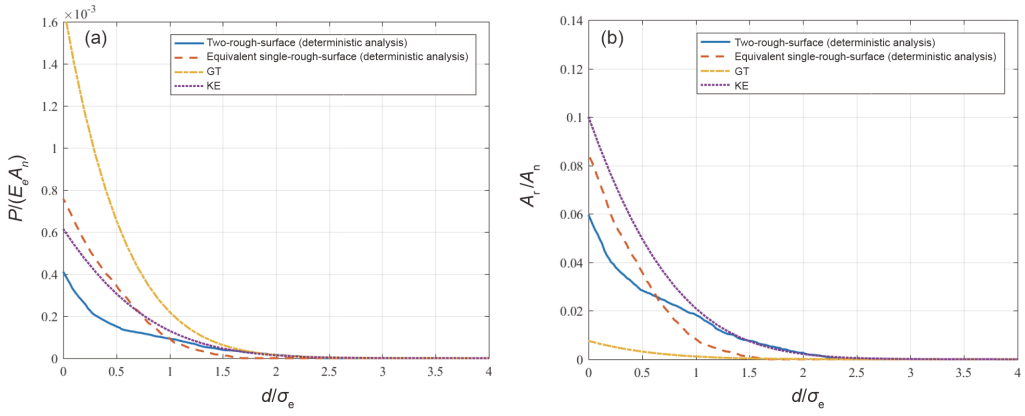

Figure 22 (Color online) Deterministic analysis in case B. (a) Dimensionless contact load versus dimensionless separation; (b) contact area ratio versus dimensionless separation.

to 1. This phenomenon is corresponding to the deterministic contact area ratio in Figure 21(b). As shown in Figure 21(b), when the dimensionless separation reduces to 1, the contact area ratio has a small mutation as well. It is hard for the model-based methods to predict this kind of "special" situation because some information has been omitted.

5 Deterministic contact analysis

5.1 Deterministic two-rough-surface contact and deterministic equivalent single-rough-surface contact

Engineering contact is a two-rough-surface contact problem, in which both the surfaces are rough. So the deterministic two-rough-surface contact is theoretically more in line with the actual situation. However, in traditional model-based methods, the equivalent single-rough-surface contact is more frequently used. Here the deterministic two-rough-surface contact and the deterministic equivalent single-rough-surface contact will be compared and analyzed. Considering results of the deterministic rough surface contact at three different cases have similar tendency, this section takes the rough surface contact shown in Figure 19 as an example for analysis.

It can be seen from Figure 20(a) that at the early stage of contact, the dimensionless contact load of the deterministic two-rough-surface contact is slightly higher than that of the deterministic equivalent single-rough contact. It is similar for the contact area ratio in Figure 20(b). This phenomenon can be illustrated in Figure 23(a) and (b) where the equivalent contact stress nephogram is given. At the later contact stage, the dimensionless contact load of the deterministic two-rough-surface contact is gradually smaller than that of the deterministic equivalent single-rough-surface contact. As shown in Figure 23(c)–(f), when the separation is reduced, the contact area ratio of the equivalent single-rough-surface is gradually larger than that of the two-rough-surface contact. Meanwhile, the region with plastic deformation is larger in the deterministic equivalent single-rough-surface contact analysis.

The solid results of the bottom body of the two kinds of deterministic rough surface contact at d/σ_e=0 are also given in Figure 24.

5.2 Deterministic contact analysis between surfaces with similar statistic parameters

In the classic model-based contact methods, some statistic parameters such as η, β and σ are adopted to express the rough surfaces. So the contact results for different pair of rough surfaces with similar statistic parameters will be similar. However, the roughness distribution is not considered in the model-based methods. This may lead to different results in different contact cases even the statistic parameters are similar. Here the deterministic two-rough-surface contact will be used to check the effects of the roughness distribution. Besides, considering the practice engineering applications, the separation D based on the surface height is used in this section.

Figure 25 shows the generated 3D rough surfaces with similar roughness parameters, which are listed in Table 7. However, the roughness distribution of different surfaces will be quite different, because the surfaces are generated randomly. For simplicity, the two same surfaces are used to conduct the deterministic two-rough-surface contact analysis.

Figure 26 shows the dimensionless contact load versus the dimensionless separation after a deterministic two-rough-surface contact analysis. There is little difference at the early stage of contact. However, as the separation between two surfaces decreases, the difference gradually increases. It can also be seen in Figure 27, when the separation between the

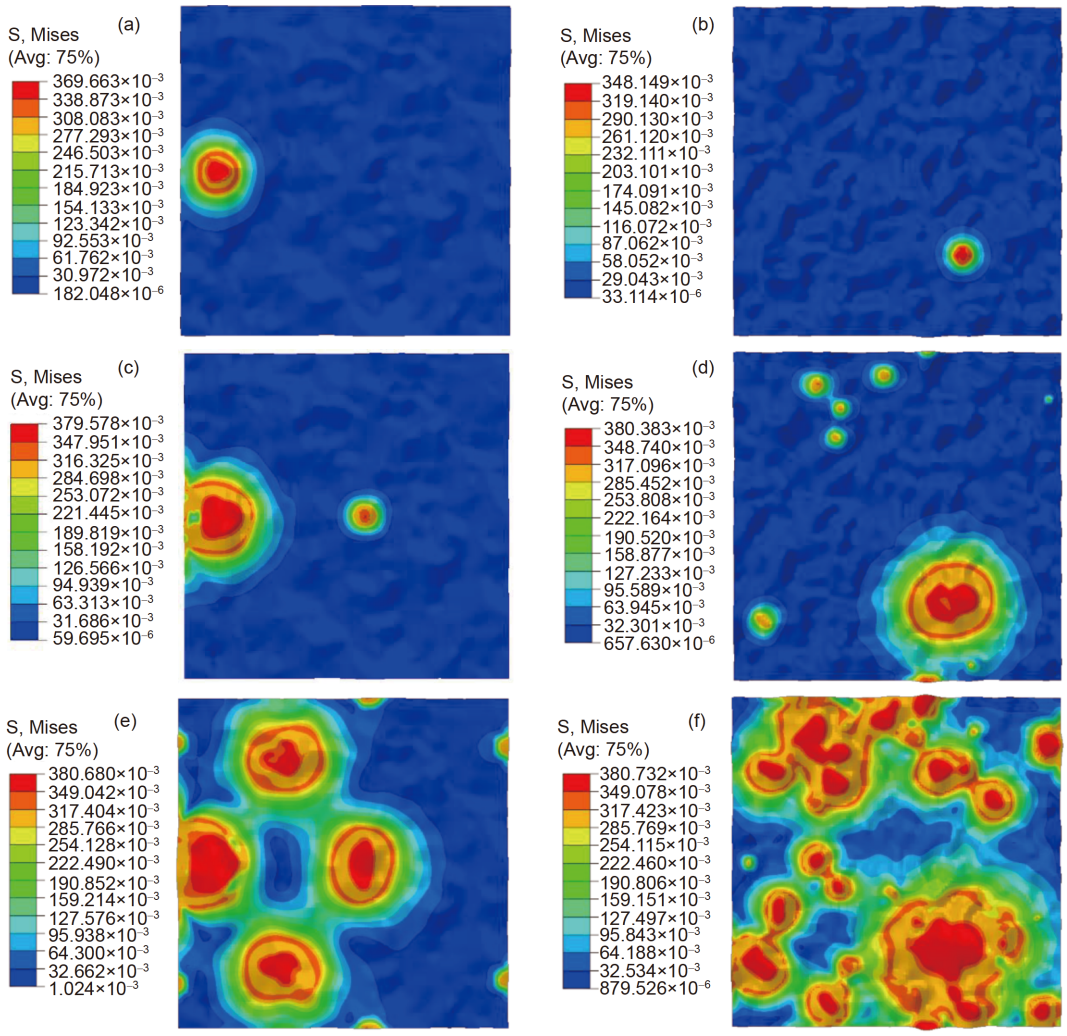

Figure 23 (Color online) Equivalent stress nephogram (GPa) of deterministic contact. (a) Two-rough-surface at d/σ_e=2; (b) equivalent single-rough-surface at d/σ_e=2; (c) two-rough-surface at d/σ_e=1; (d) equivalent single-rough-surface at d/σ_e=1; (e) two-rough-surface at d/σ_e=0; (f) equivalent single-rough-surface at d/σ_e=0.

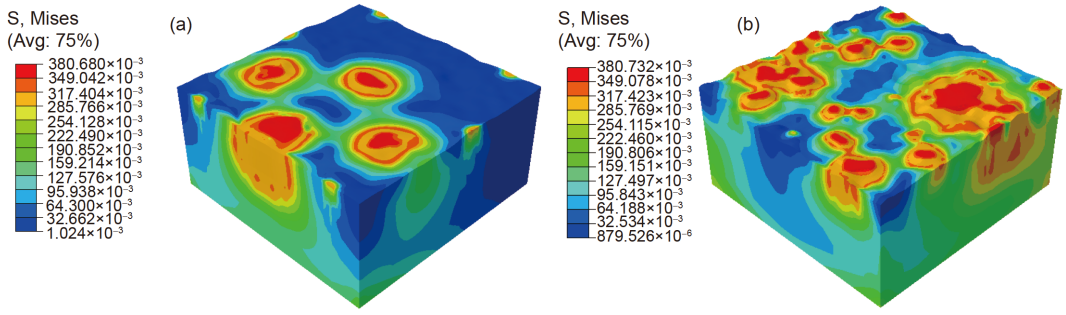

Figure 24 (Color online) Equivalent stress nephogram (GPa) of the bottom body. (a) Two-rough-surface at d/σ_e=0; (b) equivalent single-rough-surface at d/σ_e=0.

two rough surfaces becomes smaller, the contact regions and equivalent stress distribution of each group are significantly different. In this situation, the relationship between contact load and separation of each group is more dependent on its specific roughness distribution.

The relationship curve of the contact area ratio and the dimensionless separation is shown in Figure 28, which has a similar trend to the curve in Figure 26. At the early stage of contact, there is a little difference. With the decrease of separation, the difference in contact area ratio gradually in-

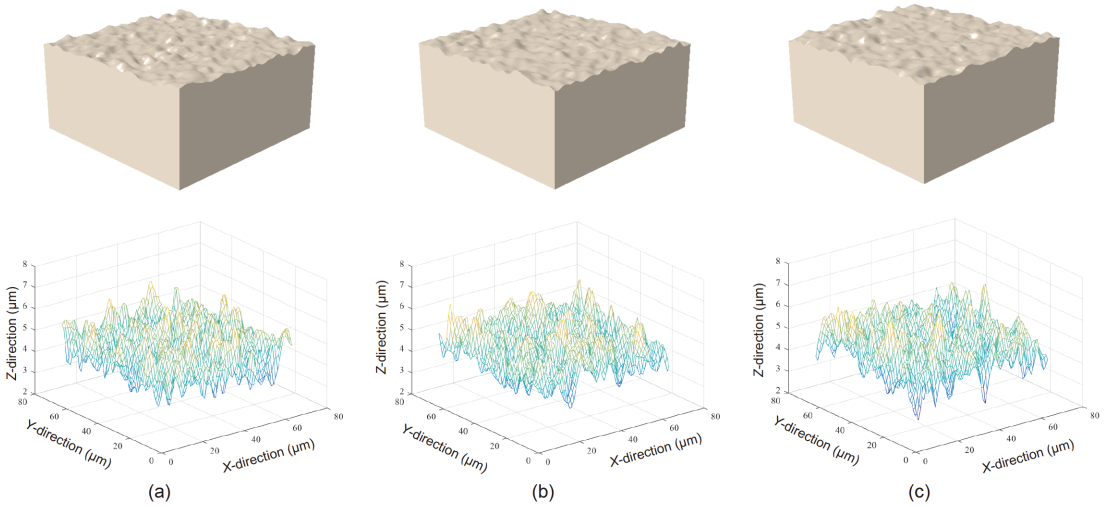

Figure 25 (Color online) 3D rough surfaces with similar roughness parameters. (a) σ=0.5437 μm, β=2.6066 μm, η=19148 mm^{-2}; (b) σ=0.5428 μm, β=2.6077 μm, η=19400 mm^{-2}; (c) σ=0.5428 μm, β=2.6060 μm, η=19148 mm^{-2}.

Table 7 Summary of surface parameters for groups 1–3

Group	σ (μm)	β (μm)	η (mm^{-2})	$\Delta\sigma$ (μm)	$\Delta\beta$ (μm)	$\Delta\eta$ (mm^{-2})
1	0.5437	2.6066	19148	–	–	–
2	0.5428	2.6077	19400	0.02%	0.04%	2.73%
3	0.5428	2.6060	19148	0.02%	0.02%	0.00%

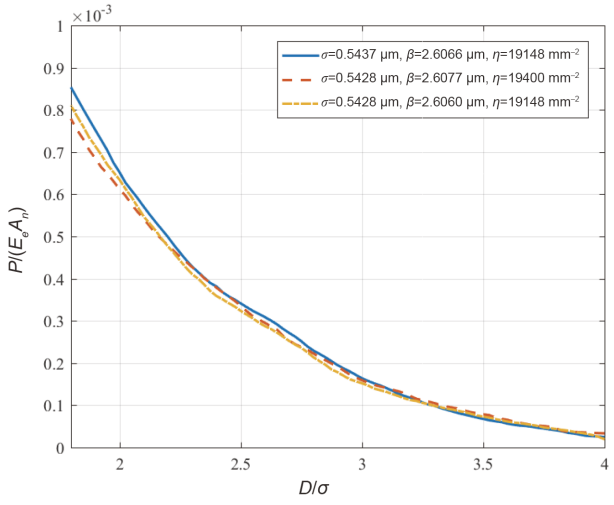

Figure 26 (Color online) Comparison of dimensionless contact load versus dimensionless separation.

creases, which also confirms that the roughness distribution is significant in the contact analysis.

5.3 Deterministic contact analysis considering multi-scale features

Most engineering surfaces have multi-scale features, in which both the roughness and textures are included [40]. Therefore, the height distribution of the corresponding rough surface with textures becomes non-Gaussian. By introducing a dimple texture into the rough surface contact shown in Figure 19, this paper considers the multi-scale rough surface contact problem. The corresponding rough solids are shown in Figure 29. The dimple texture is located in the center of the bottom rough solid. The diameter of the dimple texture is 30 μm, and the depth is 3 μm. The detail size and location of the dimple texture can be seen in Figure 6.

At first, the deterministic contact results of the two-rough-surface are analyzed. As shown in Figure 30(a), after the introduction of the texture, the relationship between the dimensionless contact load and the dimensionless separation changes little at the initial contact stage. With the decrease of separation, the dimensionless contact load of the surface with texture is gradually smaller than that of the surface without texture. As the separation between two rough surfaces decreases, the difference gradually increases. Figure 31 presents the equivalent stress nephogram of the two-rough-surface contact. As shown in Figure 31(a), (c), and (e), the equivalent stress in the central region, in which the dimple texture is located, is large. Therefore, where the dimple texture exists belongs to the primary contact region. After the introduction of the texture, the central region is no longer in contact. So, as shown in Figure 30(b), the contact area ratio of the surface with texture decreases. The corresponding

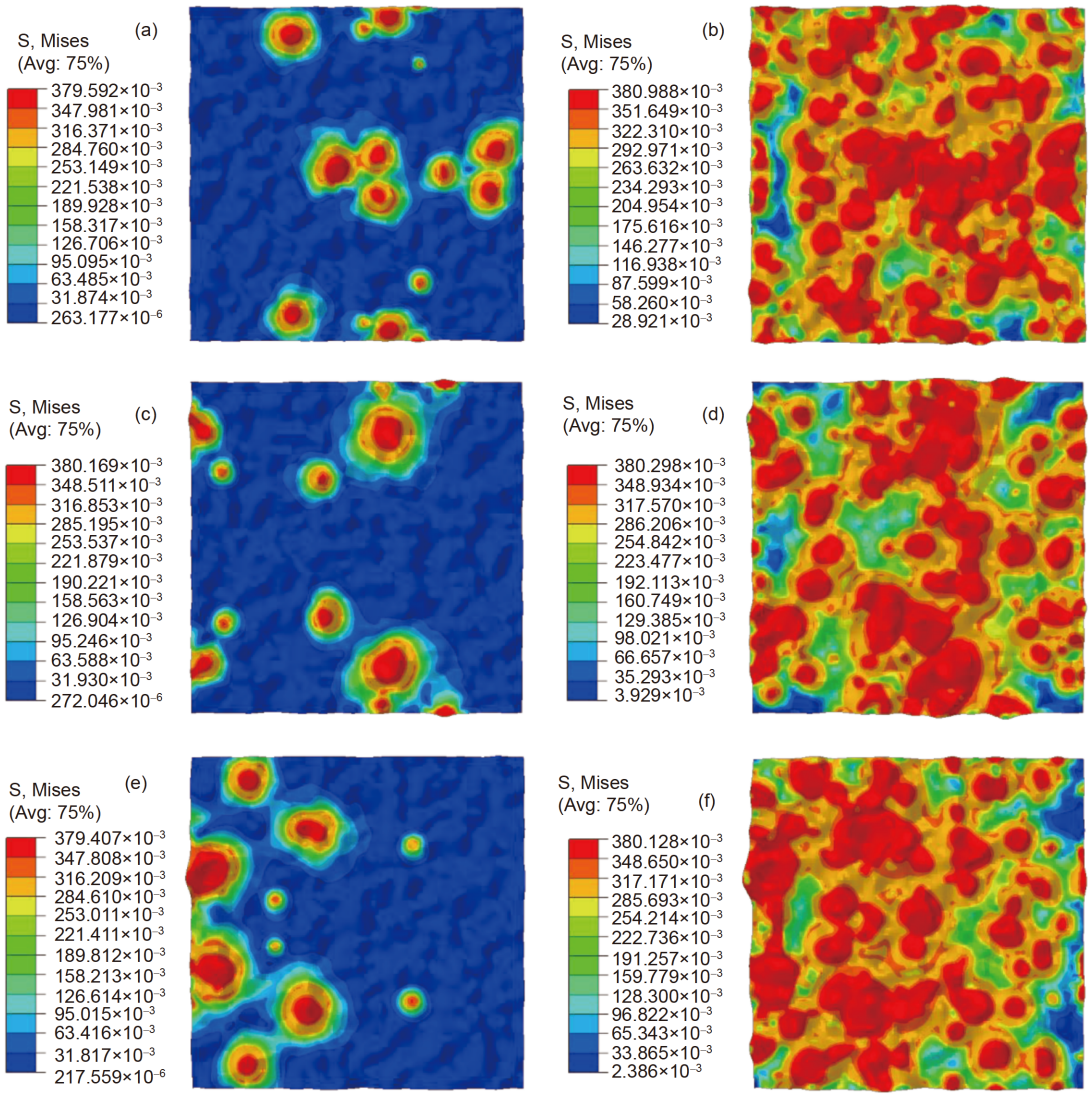

Figure 27 (Color online) Equivalent stress nephogram (GPa) of groups 1–3. (a) Group 1 at D/σ=3; (b) group 1 at D/σ=1; (c) group 2 at D/σ=3; (d) group 2 at D/σ=1; (e) group 3 at D/σ=3; (f) group 3 at D/σ=1.

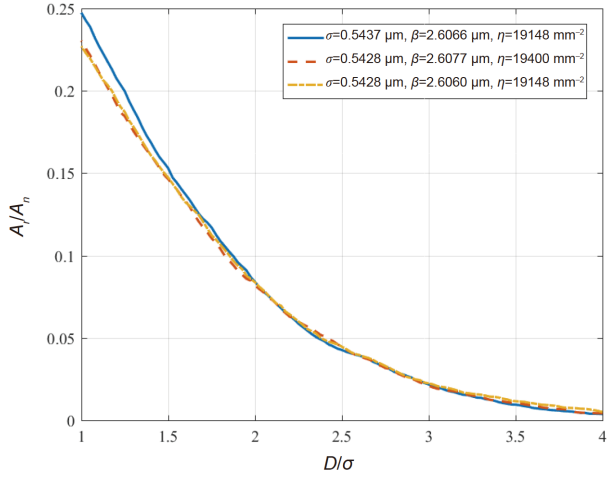

Figure 28 (Color online) Comparison of contact area ratio versus dimensionless separation.

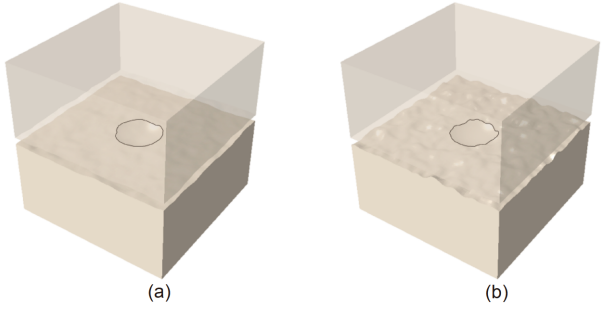

Figure 29 (Color online) 3D rough solids. (a) Two-rough-surface with texture; (b) equivalent single-rough-surface with texture.

dimensionless contact load also decreases for the reduction of interference. As two rough surfaces get closer, the influence of the dimple texture gradually increases. Therefore, the

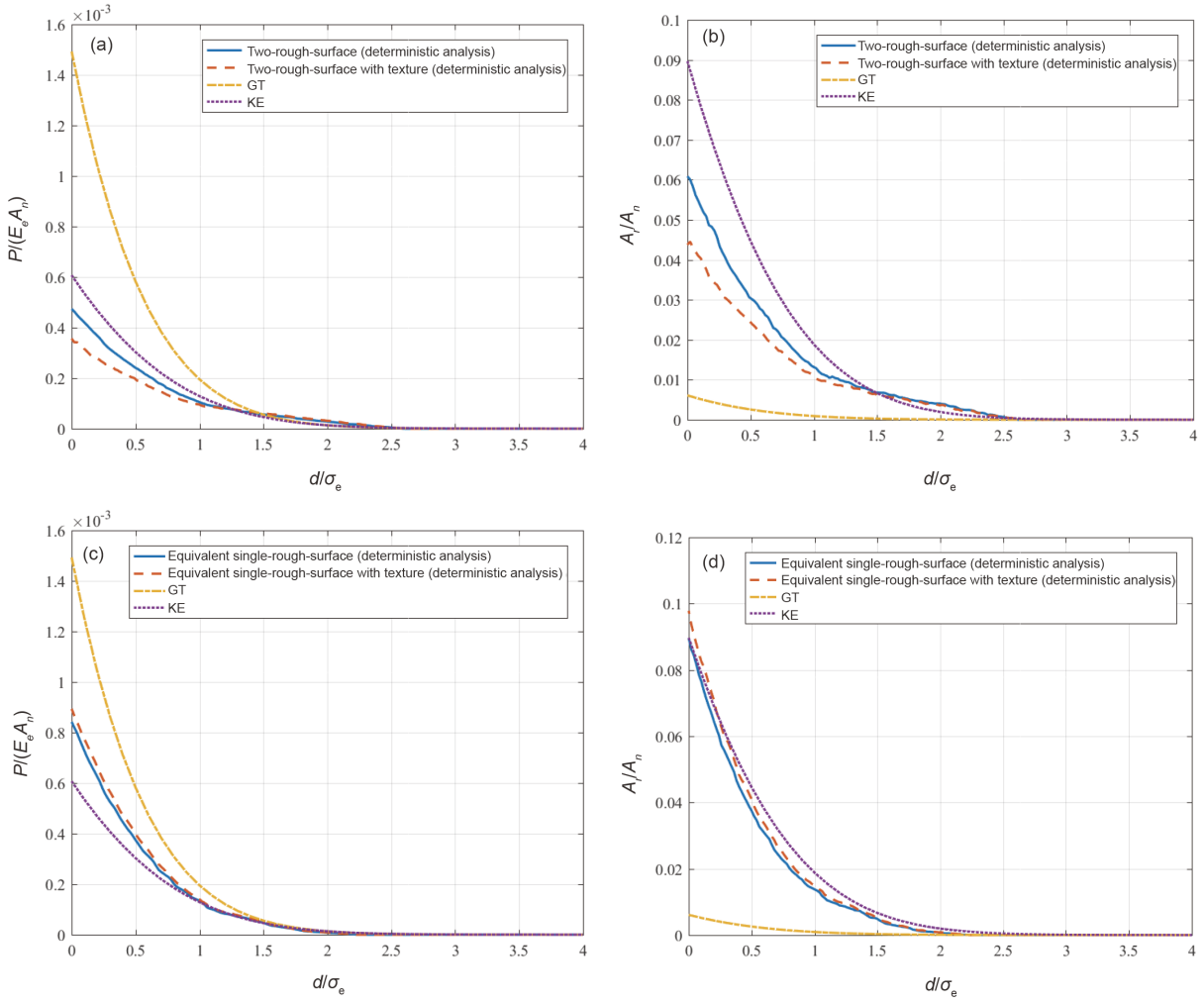

Figure 30 (Color online) (a) Comparison of dimensionless contact load versus dimensionless separation; (b) comparison of contact area ratio versus dimensionless separation; (c) comparison of dimensionless contact load versus dimensionless separation; (d) comparison of contact area ratio versus dimensionless separation.

difference between two-rough-surface without texture and two-rough-surface with texture becomes more significant.

Then, the contact results of the equivalent single-rough-surface are also analyzed. As shown in Figure 30(c), after the introduction of texture, it is interesting to find that there is no significant change. Figure 32 presents the equivalent stress nephogram of the equivalent single-rough-surface. Combined with the equivalent stress nephogram, it can be found that the equivalent stress of the central region is small. By comparing Figures 31 and 32, we can see that the texture is not at the main contact region for the equivalent rough surface contact. Therefore, after the introduction of the texture, the change of the dimensionless contact load is not significant. However, as shown in Figure 30(d), because the existence of the texture, the contact area ratio of the textured situation increased slightly compared with the non-texture situation.

To sum up, the influence of texture on the contact of rough surfaces is not simply the increase of mean contact pressure, the decrease of contact area ratio or vice versa, but is related to the specific distribution of multi-scale features. Therefore, the prediction results of classic model-based methods such as the GT model and KE model are even less applicable for the multi-scale rough surfaces. In this case, the multi-scale deterministic contact model shows its significance and should be introduced. Besides, this conclusion can be obtained by differences between the two-rough-surface contact and the equivalent single-rough-surface contact: two-rough-surface contact cannot be equal to its equivalent single-rough-surface contact when there exist textures.

6 Conclusion

Considering the distribution of multi-scale features, including roughness and textures, this paper has conducted a de-

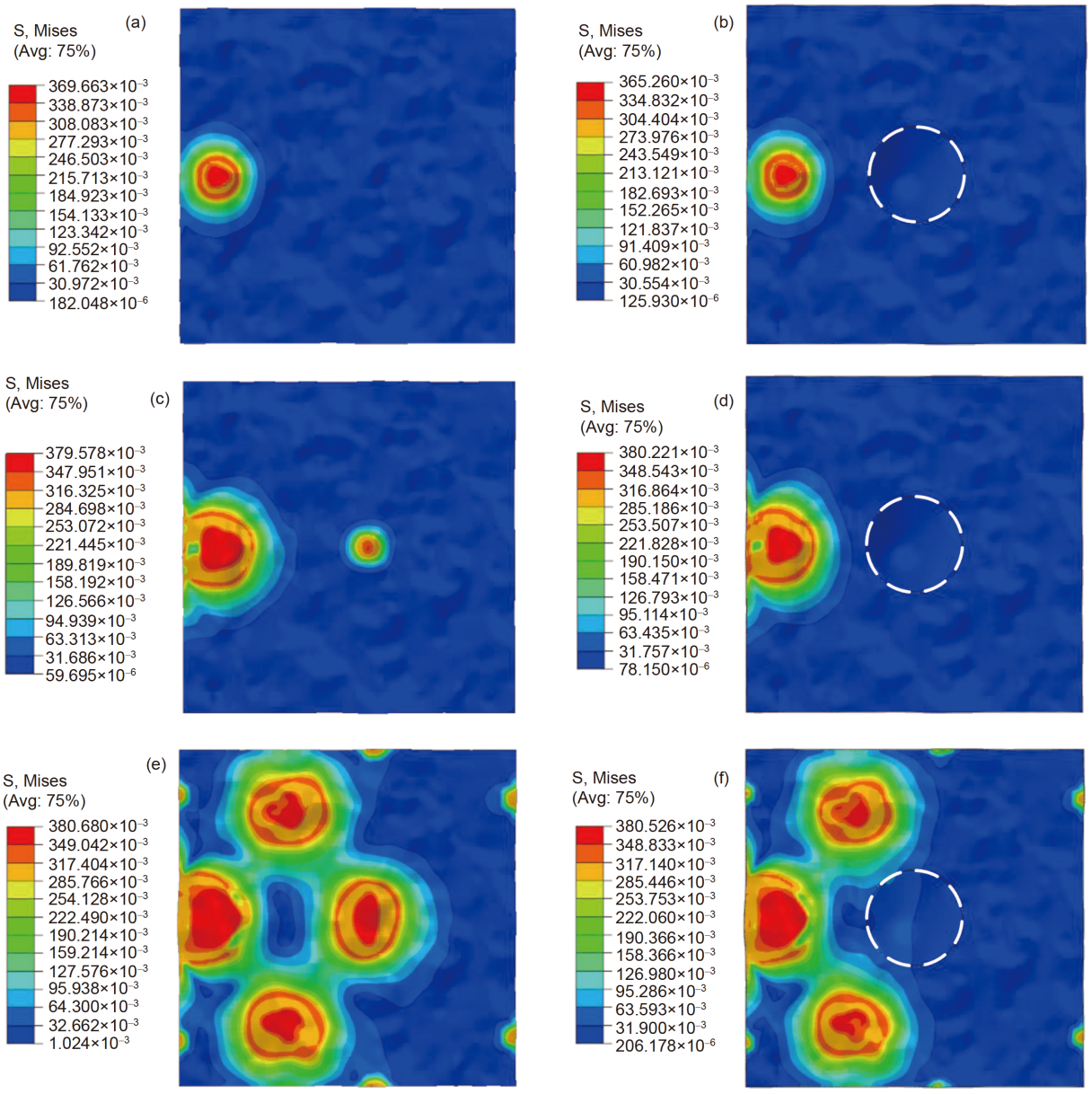

Figure 31 (Color online) Comparison of equivalent stress nephogram (GPa). (a) Two-rough-surface at d/σ_e=2; (b) two-rough-surface with texture at d/σ_e=2; (c) two-rough-surface at d/σ_e=1; (d) two-rough-surface with texture at d/σ_e=1; (e) two-rough-surface at d/σ_e=0; (f) two -rough-surface with texture at d/σ_e=0.

terministic analysis of the multi-scale 3D rough surfaces contact problem. The results have been compared with those of the classic GT model and KE model. The following conclusions can be obtained.

(1) At the early stage of contact, the results of the classic GT model and the KE model are very close to the deterministic results. However, with the decrease of the separation between two contact surfaces, the difference becomes very big, although the KE model is more accurate than the GT model for the former considers the plastic contact. So the specific roughness distribution should be considered in the contact calculation.

(2) Through the deterministic contact analysis, it can be seen that the difference between the two-rough-surface contact and the equivalent single-rough-surface contact is significant, especially for the later contact stage. Considering that the two-rough-surface contact is more consistent with the actual situation theoretically, it is essential to use this kind of contact analysis when dealing with practical engineering problems.

(3) The distribution of multi-scale topographic features, including the roughness distribution and the texture distribution, is significant for the contact analysis. The multi-scale features will lead to very different results and should be considered during the contact calculation of engineering surfaces.

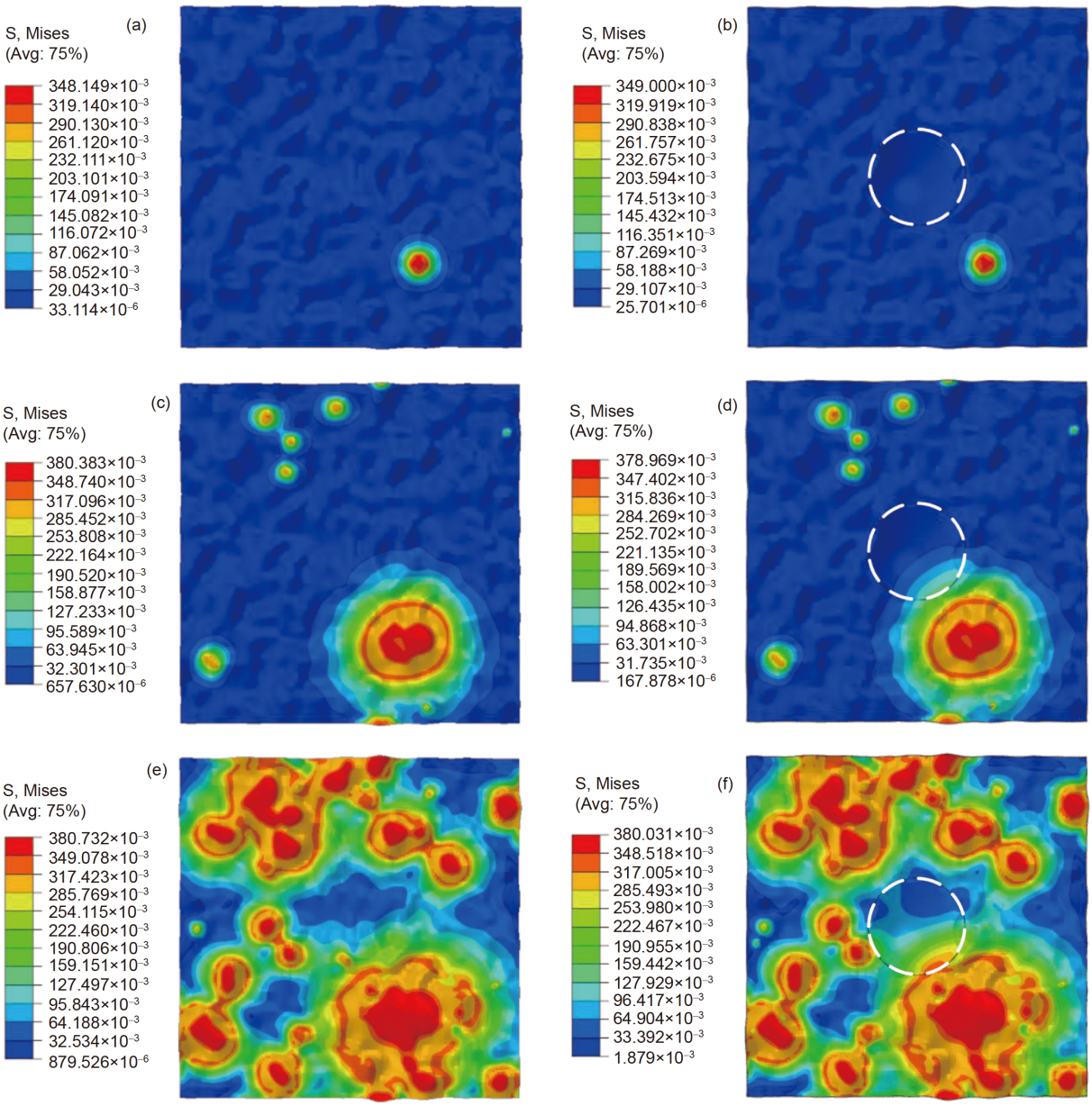

Figure 32 (Color online) Comparison of equivalent stress nephogram (GPa). (a) Equivalent single-rough-surface at d/σ_e=2; (b) equivalent single-rough-surface with texture at d/σ_e=2; (c) equivalent single-rough-surface at d/σ_e=1; (d) equivalent single-rough-surface with texture at d/σ_e=1; (e) equivalent single-rough-surface at d/σ_e=0; (f) equivalent single-rough-surface with texture at d/σ_e=0.

This paper mainly considers the influence of the multi-scale topographic features of the surface and its distribution on the contact calculation. In fact, if considering the properties of the surface materials, especially when considering the surface physical adsorption membrane, the chemical reaction membrane, the basic materials and their difference, the contact situation will become more complicated. These factors' influences will be carried out in future studies.

This work was supported by the National Natural Science Foundation of China (Grant No. 51875344 & 51705492).

Supporting Information

The supporting information is available online at tech.scichina.com and link.springer.com. The supporting materials are published as submitted, without typesetting or editing. The responsibility for scientific accuracy and content remains entirely with the authors.

1 Greenwood J A, Williamson J B P. Contact of nominally flat surfaces. Proc R Soc Lond A, 1966, 295: 300–319
2 Hertz H. Über die Berührung fester elastischer Körper und über die Harte. Gesammelte Werke Bd, 1882, 1: 156–171
3 Greenwood J A, Tripp J H. The elastic contact of rough spheres. J Appl Mech, 1967, 34: 153–159
4 Chang W R, Etsion I, Bogy D B. An elastic-plastic model for the

contact of rough surfaces. J Tribol, 1987, 109: 257–263
5 Kogut L, Etsion I. Elastic-plastic contact analysis of a sphere and a rigid flat. J Appl Mech, 2002, 69: 657–662
6 Kogut L, Etsion I. A finite element based elastic-plastic model for the contact of rough surfaces. Tribol Trans, 2003, 46: 383–390
7 Majumdar A, Bhushan B. Fractal model of elastic-plastic contact between rough surfaces. J Tribol, 1991, 113: 1–11
8 Persson B N J. Contact mechanics for randomly rough surfaces. Surf Sci Rep, 2006, 61: 201–227
9 Jackson R L, Streator J L. A multi-scale model for contact between rough surfaces. Wear, 2006, 261: 1337–1347
10 Miao X, Huang X. A complete contact model of a fractal rough surface. Wear, 2014, 309: 146–151
11 Li R, Meng X, Xie Y. A new coupling tribodynamic model of crosshead slipper-guide system and piston skirt-liner system of low-speed marine diesel engines. Tribol Int, 2018, 117: 189–205
12 Sadeghi F, Jalalahmadi B, Slack T S, et al. A review of rolling contact fatigue. J Tribol, 2009, 131: 041403
13 Lu W, Thouless M D, Hu Z, et al. CASL structural mechanics modeling of grid-to-rod fretting (GTRF). JOM, 2016, 68: 2922–2929
14 Chen W W, Liu S, Wang Q J. Fast Fourier transform based numerical methods for elasto-plastic contacts of nominally flat surfaces. J Appl Mech, 2008, 75: 011022
15 Zhang S, Wang W, Zhao Z. The effect of surface roughness characteristics on the elastic-plastic contact performance. Tribol Int, 2014, 79: 59–73
16 Zhao B, Zhang S, Keer L M. Semi-analytical and numerical analysis of sliding asperity interaction for power-law hardening materials. Wear, 2016, 364-365: 184–192
17 Nyqvist J, Kadiric A, Ioannides S, et al. Semi-analytical model for rough multilayered contacts. Tribol Int, 2015, 87: 98–112
18 Peng W, Bhushan B. Transient analysis of sliding contact of layered elastic/plastic solids with rough surfaces. Microsyst Technol, 2003, 9: 340–345
19 Bemporad A, Paggi M. Optimization algorithms for the solution of the frictionless normal contact between rough surfaces. Int J Solids Struct, 2015, 69-70: 94–105
20 Rey V, Anciaux G, Molinari J F. Normal adhesive contact on rough surfaces: Efficient algorithm for FFT-based BEM resolution. Comput Mech, 2017, 60: 69–81
21 Jackson R L, Green I. A finite element study of elasto-plastic hemispherical contact against a rigid flat. J Tribol, 2005, 127: 343–354
22 Andersen D H, Zhang Z L. Contact area on rough surface of nonlinear isotropic brittle materials. Wear, 2011, 271: 1017–1028
23 Angadi S V, Jackson R L, Choe S, et al. A multiphysics finite element model of a 35A automotive connector including multiscale rough surface contact. J Electron Packag, 2012, 134: 011001
24 Wagner P, Wriggers P, Klapproth C, et al. Multiscale FEM approach for hysteresis friction of rubber on rough surfaces. Comput Methods Appl Mech Eng, 2015, 296: 150–168
25 Zhao B, Zhang S, Qiu Z. Analytical asperity interaction model and numerical model of multi-asperity contact for power hardening materials. Tribol Int, 2015, 92: 57–66
26 Bakolas V. Numerical generation of arbitrarily oriented non-Gaussian three-dimensional rough surfaces. Wear, 2003, 254: 546–554
27 Wu J J. Simulation of rough surfaces with FFT. Tribol Int, 2000, 33: 47–58
28 Wu J J. Simulation of non-Gaussian surfaces with FFT. Tribol Int, 2004, 37: 339–346
29 Sahoo P, Ghosh N. Finite element contact analysis of fractal surfaces. J Phys D-Appl Phys, 2007, 40: 4245–4252
30 Pei L, Hyun S, Molinari J F, et al. Finite element modeling of elasto-plastic contact between rough surfaces. J Mech Phys Solids, 2005, 53: 2385–2409
31 Poulios K, Klit P. Implementation and applications of a finite-element model for the contact between rough surfaces. Wear, 2013, 303: 1–8
32 An B, Wang X, Xu Y, et al. Deterministic elastic-plastic modelling of rough surface contact including spectral interpolation and comparison to theoretical models. Tribol Int, 2019, 135: 246–258
33 Poon C Y, Bhushan B. Numerical contact and stiction analyses of Gaussian isotropic surfaces for magnetic head slider/disk contact. Wear, 1996, 202: 68–82
34 Hu Y Z, Tonder K. Simulation of 3D random rough surface by 2-D digital filter and Fourier analysis. Int J Machine Tools Manufacture, 1992, 32: 83–90
35 Fang C, Meng X, Xie Y. A piston tribodynamic model with deterministic consideration of skirt surface grooves. Tribol Int, 2017, 110: 232–251
36 Shi X, Zou Y. A comparative study on equivalent modeling of rough surfaces contact. J Tribol, 2018, 140: 041402
37 Reichert S, Lorentz B, Albers A. Influence of flattening of rough surface profiles on the friction behaviour of mixed lubricated contacts. Tribol Int, 2016, 93: 614–619
38 Kucharski S, Starzynski G. Study of contact of rough surfaces: Modeling and experiment. Wear, 2014, 311: 167–179
39 Greenwood J A, Tripp J H. The contact of two nominally flat rough surfaces. Proc Inst Mech Eng, 1970, 185: 625–633
40 Gu C, Meng X, Xie Y, et al. Effects of surface texturing on ring/liner friction under starved lubrication. Tribol Int, 2016, 94: 591–605